Comparison of TiO_2 and ZnO electron selective layers on the inverted-type polymer solar cells

İdris Candan & Yunus Özen

Polymer Bulletin

ISSN 0170-0839
Volume 78
Number 6

Polym. Bull. (2021) 78:3117-3129
DOI 10.1007/s00289-020-03271-8

Springer

Your article is protected by copyright and all rights are held exclusively by Springer-Verlag GmbH Germany, part of Springer Nature. This e-offprint is for personal use only and shall not be self-archived in electronic repositories. If you wish to self-archive your article, please use the accepted manuscript version for posting on your own website. You may further deposit the accepted manuscript version in any repository, provided it is only made publicly available 12 months after official publication or later and provided acknowledgement is given to the original source of publication and a link is inserted to the published article on Springer's website. The link must be accompanied by the following text: "The final publication is available at link.springer.com".



Author's personal copy

Polymer Bulletin (2021) 78:3117–3129
https://doi.org/10.1007/s00289-020-03271-8

ORIGINAL PAPER

Comparison of TiO_2 and ZnO electron selective layers on the inverted-type polymer solar cells

İdris Candan[1] · Yunus Özen[2,3]

Received: 27 September 2019 / Revised: 29 May 2020 / Accepted: 12 June 2020 /
Published online: 18 June 2020
© Springer-Verlag GmbH Germany, part of Springer Nature 2020

Abstract

In this study, P3HT:PCBM polymer-based solar cell devices with TiO_2 and ZnO electron selective layers were separately investigated to compare effects of metal oxide layer in the inverted-type polymer solar cell structures. R.f. magnetron sputtering technique was used to fabricate highly oriented polycrystalline TiO_2 and ZnO thin film layers onto FTO-coated glass substrates. The surface morphology, structural and optical properties of TiO_2 and ZnO electron selective layers were studied by performing X-ray diffraction (XRD), confocal Raman spectroscopy, transmittance spectra and Atomic Force Microscope (AFM). Photovoltaic performance of inverted-type polymer solar cell based on Poly (3-hexylthiophene-2,5-diyl) (P3HT) and [6,6]-Phenyl C61 butyric acid methyl ester (PCBM) with different electron selective layers was executed to analyze the effects of TiO_2 and ZnO thin film layers on the power conversion efficiency (PCE) value of inverted polymer solar cell (IPSC) devices. Produced devices with TiO_2 and ZnO thin film indicated the best device performance with maximum PCE values of 2.88 and 3.49%, respectively.

Introduction

Semiconducting polymer materials as a photoactive layer have attracted considerable interests for photovoltaic (PV) solar cell device applications as an alternative energy source due to simple/fast roll-to-roll production and their potential for low cost materials since their discovery in 1985 [1–4]. Polymer photoactive layer can be coated by using solution processing on flexible substrates at room temperature. Furthermore, conjugated polymers exhibit higher absorption extinction coefficients than inorganic materials and provide more effective light harvesting [5, 6]. Generally,

✉ İdris Candan
idris.candan@kocaeli.edu.tr

1 Department of Physics, Kocaeli University, 41001 Izmit, Kocaeli, Turkey

2 Department of Physics, Faculty of Science, Gazi University, 06500 Ankara, Turkey

3 Photonics Application and Research Center, Gazi University, 06500 Ankara, Turkey

Author's personal copy

polymer active layers are made of at least two different organic-based materials having different electron affinity or mixture of polymer and fullerene materials in bulk (bulk heretojunction metarial, BHJ) [7, 8]. The polymer donor with low electron affinity gives electrons to fullerene acceptor with high electron affinity under illumination [9]. The structure of BHJ supplies more efficient charge separation and a larger place of pathways for the carrying of separated free carriers (electrons and holes) compared to the other structures [10]. Power conversion efficiencies (PCE) of over 15.5% has recently achieved for solution-processed single-layer of PM6:Y6/PDINO based BHJ and has reached up to 17.3% for the PTB7-Th:O6T-4F with $PC_{71}BM$ based tandem solar cells composed of multiple BHJs organic photovoltaic (OPV) solar cells [11, 12]. Among polymer-based solar energy harvesting materials, Poly (3-hexylthiophene-2,5-diyl) (P3HT) as a donor semiconductor (p-type) and [6,6] -Phenyl C61 butyric acid methyl ester (PCBM) as an electron acceptor conducting material (n-type) have lately become popular materials for construction of low-priced solar cells [13, 14]. Since the application of P3HT:PCBM in OPVs, different device efficiency has been reported in the literature in between 2 and 5% [15–18].The electron donor polymer (p-type) and an electron deficient fullerene based acceptor polymer (n-type) semiconductor can be blended in a bulk heterojunction (BHJ) configuration to construct polymer photoactive layer based solar cell devices [13, 19]. In the donor–acceptor interface, the excitons are generated by photons and they separate into free charge carriers of electrons and holes within a few nanometers throughout the polymer photoactive layer. These seperated electrons and holes move over the photoactive BHJ polymer layer and reach to the collector terminals creating a current. The conventional P3HT:PCBM based BHJ solar cells are manufactured with an photoactive layer inserted in between a metal with low-work function such as aluminum (Al) acting as a cathode and hole selective layer of poly (3,4 ethylenedioxylenethiophene):poly (styrene sulfonic acid) (PEDOT:PSS) acting as an anode [4, 20, 21]. The hole selective layer of PEDOT:PSS is generally deposited on top of an anode such as ITO or FTO covered glasses [20, 21]. On the other hand, the conventional BHJ structure has a disadvantage in terms of attaining long term durability due to the oxidation problem of low-work function metal cathode layer (mostly Al), which enables penetration of oxygen to the photoactive layer and therefore reduces the solar cell performance [22, 23]. In order to overcome this problem and be able to enhance the device lifetime, a powerful approach is to construct the polymer photovoltaic solar cell devices with an inverted configuration, in which a high-work function metal coated on the hole sellective layer such as MoO_3 serves as the anode and ITO or FTO acting as cathode [22]. In an inverted geometry, ITO or FTO electrode is coated with one of the metal oxide layer such as zinc oxide (ZnO), aluminum oxide (Al_2O_3) or titanium oxide (TiO_x) as electron sellective layer while a high-work function metal (i.e. Ag) is employed as an electron blocking layer and hole collecting electrode [24–27]. In the inverted geometry, TiO_2 or ZnO electron selective layer (buffer layer) performs as a layer of hole-blocking and an electron-collecting for reaching high power conversion efficiency (PCE) [28–30]. Most of the ZnO and TiO_2 thin film layers in OPVs were deposited using wet-chemical processes such as dip-coating [31], spin-coating [30] and spray pyrolysis deposition [32], mainly due to the advantages of cheap, easy to process and simple

Author's personal copy

equipment requirements. However, it is difficult to control the homogeneity of the thickness of thin films prepared by wet-chemical processes. To overcome homogeneity problem, the sputtering method, based on vacuum technology, have been used by many researchers. The sputtering method provides more freedom for modification of deposition parameters. Therefore, it is common to use the sputtered ZnO [22, 26] and TiO_2 [33–35] thin film layers as ESL on the different type organic solar cell structures. They improve the properties of interface in between electrode and photoactive layer in the inverted structure [30, 36]. The electrical conductivity values of TiO_2 thin films in the literature have been reported to change in between 0.1 and 10 $(\Omega\ cm)^{-1}$ [37, 38], while the electrical conductivity values of ZnO thin film change in between 10^1 and 10^3 $(\Omega\ cm)^{-1}$ [39, 40] changing with growth conditions. Additionally, the conduction band edge value of the ZnO thin film layer as ESL can make the appropriate energy level alignment between the lowest unoccupied molecular orbital (LUMO) of the PCBM (around −4.0 eV) and the work function of FTO layer (around 4.4 eV) [28, 41–43]. Therefore, the energy level alignment between the work function of FTO and the LUMO of the PCBM using the ZnO layer provides a more suitable energy level for a more effective injection of electrons into the FTO layer compared to using TiO_2 layer or FTO on its own [41]. Generally, IPCSs with ZnO thin film layer exhibit higher value of PCE than IPSCs with TiO_2 thin film layer [44].

In this paper, we investigate the difference between TiO_2 and ZnO electron sellective layers (ESL) in the IPSCs. We fabricated two different IPSCs with different electron sellective thin film layers by using sputtering technique, namely, FTO/TiO_2/P3HT:PCBM/MoO_3/Ag and FTO/ZnO/P3HT:PCBM/MoO_3/Ag to compare the effects of sputtered TiO_2 and ZnO layers.

Experimental details

The inverted configuration of polymer-based solar cell devices with TiO_2 and ZnO electron-collecting buffer layer of Glass/FTO/Metal oxide/P3HT:PCBM/MoO_3/Ag have been deposited separately to compare the effects of metal oxide type used as buffer layer as seen in Fig. 1. The TiO_2 and ZnO layer were fabricated onto the FTO-coated glasses by using sputtering method. Nanovak NVTS500 co-sputtering system was separately used to deposite the TiO_2 and ZnO layers under the argon (Ar) atmosphere with pressure of 10^{-6} Torr at room temperature. In order to provide the better crystallinity in the structure of TiO_2 and ZnO thin films and supply the thermal energy to the component elements to make the nucleation stage complete with thermal kinetics in the deposited samples, post-annealing process was carried out for the thin films at temperature of 250 °C for 1 h under the nitrogen (N_2) atmosphere. The thickness of produced TiO_2 and ZnO samples were determined in between 40 and 50 nm by using profilometer of Veeco Dektak 150 stylus type.

Commercially purchased P3HT (Sigma-Aldrich (CAS Number: 156074-98-5) with number average molecular weight (M_w): 45,000–65,000 g mol^{-1} and polydispersity index (PDI) of ~ 2) and PCBM (with wt-ratio of 1:1) were dissolved in Dichlorobenzene (DCB) solvent at 20 mg/mL concentration with magnetic stirrer at temperature of

Author's personal copy

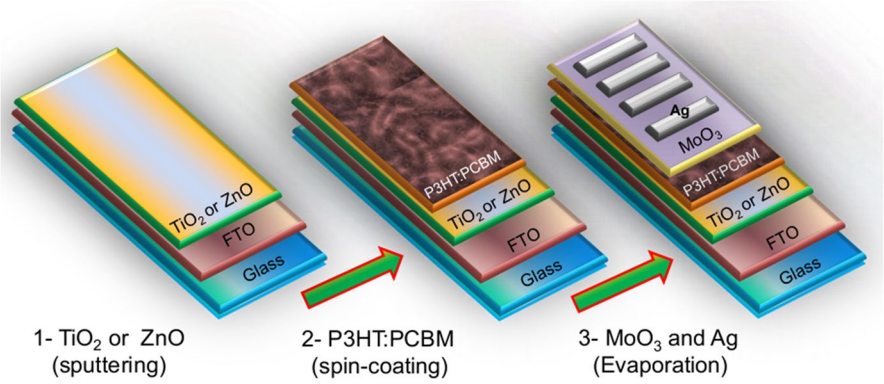


Fig. 1 Schematic demonstration of the fabrication steps of IPSC device with TiO_2 electron sellective layer of Glass/FTO/TiO_2/P3HT:PCBM/MoO_3/Ag and with ZnO electron sellective layer of Glass/FTO/ZnO/P3HT:PCBM/MoO_3/Ag inverted polymer solar cell (IPSC) structures

40 °C for 8 h. The mixture of P3HT:PCBM was covered onto the TiO_2/FTO/Glass and ZnO/FTO/Glass substrates by using spin coating technique. In addition, the polymer photoactive layer was coated on the FTO/Glass substrate to use as a reference sample. Süss Microtec 6 RC spin coater system and the parameters of 600 rpm and 1100 rpm for 20 and 9 s was used to deposit photoactive layer, respectively. Post production annealing process was then utilized to the sample at 150 °C for 5 min on the hot plate to improve the photoactive absorber layer and to evaporate the remaining solvents in the structure. The hole-collecting layer of molybdenum trioxide (MoO_3) and the top metal electrode of silver (Ag) layers were coated 10 nm and 100 nm by using the BesTec thermal evaporation system, respectively.

Transmittance spectra was carried out in between 300–1100 nm wavelength range by utilizing the spectrometer system of Perkin Elmer Lambda 2S UV–Vis–NIR. The structural properties of the deposited TiO_2 and ZnO thin film samples were analized by using Rigaku Miniflex XRD system having radiation source of CuKα (wavelength at 1.54 Å). Jobin–Yvon Horiba confocal Raman with excitation source of the 532 nm Nd:YAG laser was executed to study the confocal Raman measurements at room temperature. CCD detector with Peltier cooled and double monochromator were employed to designate Raman shifts. AFM image was obtained at room temperature by using high-performance AFM system (Nano Magnetics Instruments Ltd., Oxford, UK). A Keithley 4200 source meter were used to execute the current density as a function of applied voltage (*J*–*V*) measurements and Newport Oriel-Sol1A solar simulator was used to generate AM 1.5 G illumination.

Results and discussions

In order to examine the optical behaviors of the fabricated metal oxide electron selective layers of TiO_2 and ZnO thin film samples; transmittance measurements were executed by using UV–VIS-IR Spectroscopy. The transmittance spectra of the

Author's personal copy

glass, Glass/FTO, sputtered TiO_2 and ZnO onto FTO coated glass samples studied in the wavelength range of 300 and 1100 nm were demonstrated in Fig. 2a. As clearly seen from Fig. 2a, the transmission ratios of ZnO and TiO_2 were observed in between 70–85% and 60–78% in the wavelength range of 400 and 900 nm, respectively. Transmittance data also shows that thin films have enough transparency and allow maximum wavelengths to pass through the active polymer thin film layer and create the electron–hole pairs.

Figure 2b, c demonstrate the XRD patterns of TiO_2 and ZnO thin film samples obtained through a Rigaku Miniflex diffractometer using CuKα radiation in the range of 2θ = 10°–80°, respectively. The well-defined sharp Bragg peaks point out highly crystalline nature of the materials. As seen from Fig. 2b, the Bragg diffraction peaks at 26.7°, 37.8, 51.6° and 61.7° with preferred orientation as (101), (004), (105) and (002)/(204), are correspond to TiO_2 with tetragonal arrangement [45]. Additionally, (110), (101), (220), (301), and (321) preferentially oriented reflections peaks at 33.8°, 54.6°, 65.7° and 78.4° were observed for FTO films in XRD measurements as marked in Fig. 2b [46–48]. The XRD diffraction pattern of the sputtered ZnO layer is illustrated in Fig. 2c. The pattern given in Fig. 2c clearly reveals

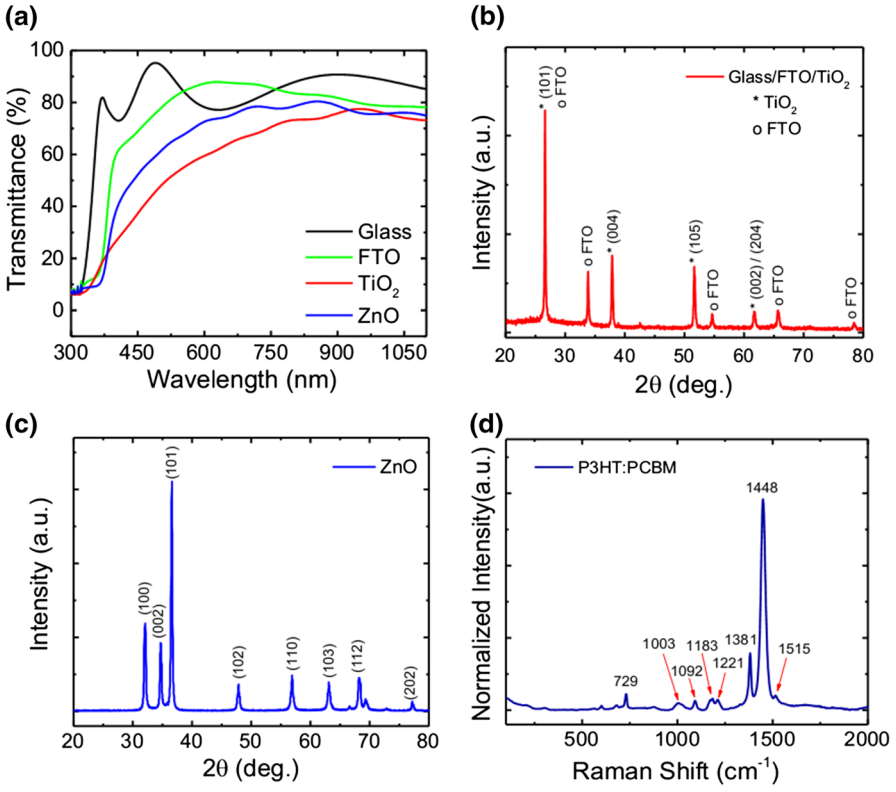


Fig. 2 **a** Transmittance (T) spectra of glass, TiO_2 and ZnO, **b** X-ray diffraction of TiO_2 and **c** X-ray diffraaction of ZnO (**d**), Raman specra of P3HT:PCBM

Author's personal copy

the polycrystalline structure with orientation along different prefered orientations. These oriantations of ZnO thin film are (100), (002), (102), (110), (103), (112), and (202) for corresponding peak positions of 32.1°, 34.7°, 47.9°, 56.9°, 63.1°, 68.2° and 77.2°, respectively [49, 50]. Furthermore, the results uncover that not only the peaks of ZnO phase but also a peak of elemental zinc (Zn) with preferred orientation of (101) at 36.6° occur [49]. The peak of Zn emerged due to Zn atomic weight being heavier than oxygen (O). An O_2 atmosphere can easily move away, leaving a higher amount of heavier argon gas in the low-pressure environment of sputtering chamber [51].

The confocal Raman spectrum of polymer thin film layer (P3HT:PCBM) was employed by operating the Nd:Yag laser with excitation source of 532 nm wavelength at room temperature and Fig. 2d indicates the results of Raman spectra. As shown in Fig. 2d, P3HT:PCBM polymer photoactive layer has the most sharp Raman peak at 1448 cm^{-1} which is allocated to the C=C symmetric stretching. Furthermore, the other Raman peaks of P3HT:PCBM active polymer layer are at 730, 1003, 1092, 1183, 1221, 1381, and 1515 cm^{-1} which are referred to the C–S–C ring deformations, C–C stretching alkyl-chain, C–H bending alkyl-chain, C–C symmetric stretching, combination of C–C stretching and C–H stretching, C–H bending, C3–C4 stretching, and C=C antisymmetric stretching, respectively [52–58].

Atomic force microscopy (AFM) was carried out to analyze the surface morphology of the fabricated TiO_2, ZnO and P3HT:PCBM thin film samples at room temperature conditions. Figure 3 exhibits the three-dimensional (3D) AFM images captured from TiO_2, ZnO and P3HT:PCBM polymer sample surfaces. The results indicate the formation of the surfaces with roughness of 9.11 nm, 13.75 nm and 5.60 nm for TiO_2, ZnO and P3HT:PCBM thin film samples, respectively. The deposition technique, parameters and conditions of sample have profound effect on the surface morphology of the fabricated thin films. As observed in XRD results, during the growth of TiO_2 and ZnO thin film layers via sputtering, the deposited layers were pre-heated at 250 °C for 1 h to enhance the crystallization of elecron sellective layers of the films. Additionally, P3HT:PCBM photoactive layer was pre-heated at 150 °C for 5 min to improve the quality of the photoactive layer and evaporate the solvent and remaining species in the photo absorber layer.

In order to build IPSC devices, two different types of selective layer (TiO_2 and ZnO) were deposited on the FTO-coated glasses by using sputtering technique to collect the electrons and blocking the holes. Figure 4 illustrates the structure and band gap positions of IPSC device and the main aim of this study. As clearly described in schematic representations, P3HT:PCBM BHJ polymer photoactive layer is inserted in between electron selective layer (TiO_2 or ZnO) and hole transport layer (MoO_3) to collect the photons from solar spectrum. In IPSC device structure, photons come from glass side and arrive at photoactive polymer layer and electron–hole pairs (excitons) are produced in the layer of blended photoactive polymer. The excitons can be divided into electrons and holes at the P3HT:PCBM interfaces and the negative and positive charge carriers are carried from polymer layer to the metal oxide (TiO_2 or ZnO) and MoO_3 layers, respectively. The incorporation of the metal oxide provides paths for the electrons while MoO_3 provides paths for the holes to pass from polymer to FTO and Ag contacts as seen from Fig. 4.

Author's personal copy

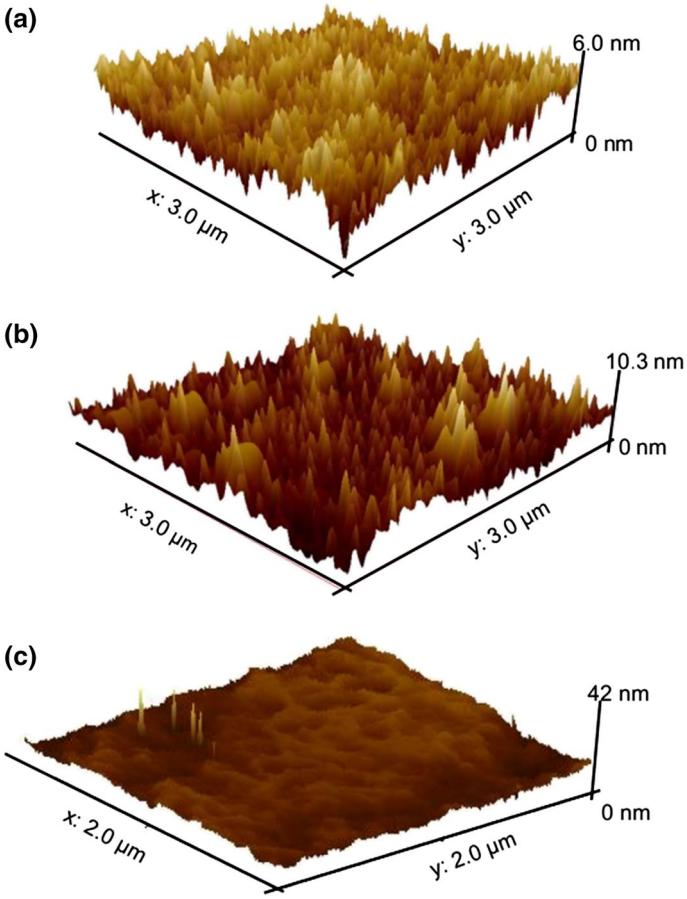


Fig. 3 AFM images of the three-dimensional (3-D) configuration of (**a**) TiO_2, (**b**) ZnO and (**c**) P3HT:PCBM thin films deposited onto the surface of FTO substrate

To compare the effects of metal oxide in the IPSC devices, current density–voltage (J–V) curves were studied under AM 1.5 G solar simulators. The performance of the IPSC without ESL and with sputtered TiO_2 and ZnO layers are shown in Fig. 5 and measured solar cell parameters of short-circuit current (J_{SC}), open-circuit voltage (V_{OC}), fill factor (FF), and power conversion efficiency (PCE) () of cells with two different electron selective layers are compared in Table 1.

The forward and reverse applied DC bias voltages varying in between -1.5 and +1.5 V under AM 1.5 G illumination were applied to carry out the characteristics of current density–voltage (J–V) of manufactured IPSC samples without ESL and with metal oxides of TiO_2 and ZnO, and results were showed in Fig. 5. The semi-logarithmic graph of J–V characteristics with sputtered TiO_2 and ZnO electron sellective layers is given as an inset of Fig. 5. As seen from the figure, the semi-logarithmic plot of forward bias current showed one order of magnitude for solar cell without ESL and two

Author's personal copy

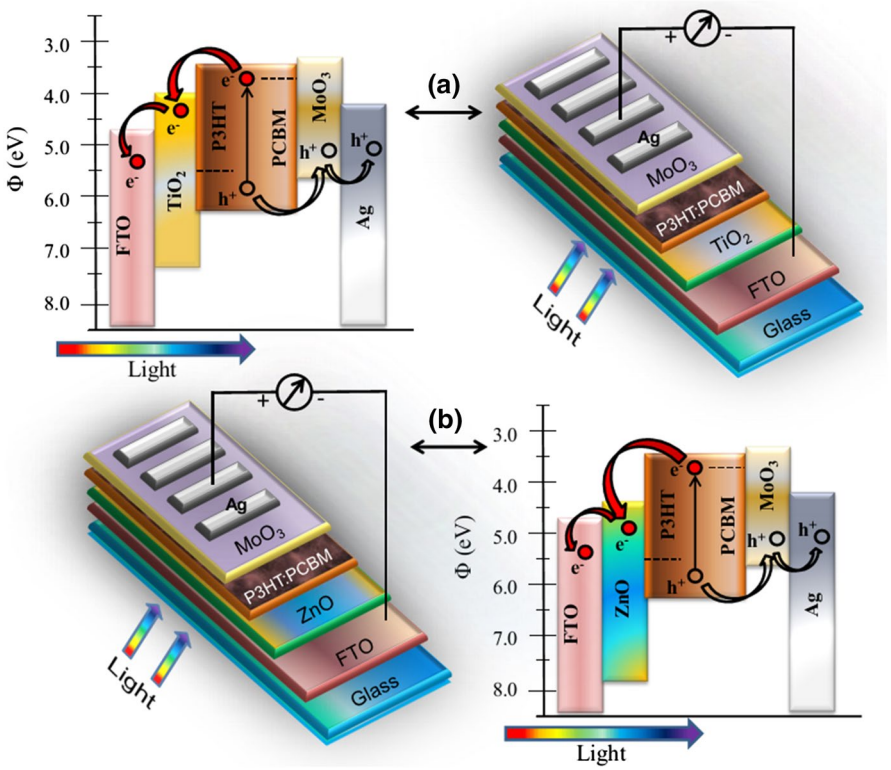


Fig. 4 Schematic representations of IPSC device (**a**) with TiO_2 thin film layer containing glass/FTO/TiO_2/P3HT:PCBM/MoO_3/Ag layers and band gap position diagram and **b** with ZnO thin film layer containing glass/FTO/TiO_2/P3HT:PCBM/MoO_3/Ag layers and band position diagram of IPSC. (The band positions of the materials have been plotted by using Refs. [20, 26and 34].)

orders of magnitude for both IPSC with ESL confugurations. The PCE value of cell without ESL was calculated as 0.13% as given in Table 1. Due to the direct coating of the photoactive layer on the FTO, the ohmic property in the structure increased and the energy conversion efficiency of the sample remained low. The electron selective layer acts as a filter and minimizes the ohmic behavior and also improves the properties of interface in between electrode and photoactive layer [28, 29, 36]. On the other hand, IPSC with sputtered TiO_2 demonstrates a PCE value around 2.88%. However, PCE was significantly increased up to 3.49% after the alteration of TiO_2 layer with sputtered ZnO layer in the device structure. This result indicated that using ZnO instead of TiO_2 thin film layer as an electron selective layer in the IPSC device geometry enhanced the performance relatively to 21%. As seen from Table 1, the device with sputtered TiO_2 layer demonstrated a J_{SC} of 9.4 mA/cm^2, V_{OC} of 0.87 V and FF of 35%, while the device with sputtered ZnO indicated a J_{SC} of 11.3 mA/cm^2, V_{OC} 0.81 V and FF of 39%. As mentioned in the introduction section, since ZnO thin film has higher electrical conductivity and can make the appropriate band alignment between P3HT:PCBM and FTO

Author's personal copy

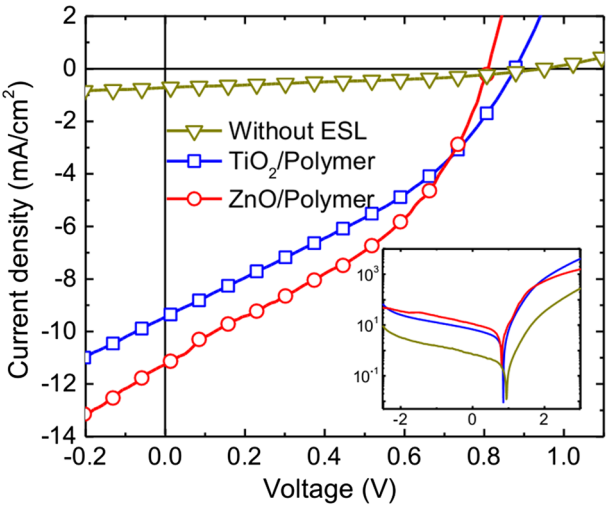


Fig. 5 The current density (*J*)–voltage (*V*) characteristics of the IPSC devices without ESL and with TiO_2 and ZnO thin film layers as ESL under illumination of AM 1.5 G. Inset is demonstrating semi-logarithmic current density–voltage characteristics of devices without ESL and with sputtered TiO_2 and ZnO metal oxide layers

Table 1 Summary of the photovoltaic performance parameters of the IPSC without ESL and with sputtered TiO_2 and ZnO electron sellective layers

Sample	J_{SC} (mA/cm^2)	V_{OC} (V)	FF (%)	η (%)
Without ESL	0.7	0.94	18	0.13
TiO_2/polymer	9.4	0.87	35	2.88
ZnO/polymer	11.3	0.81	39	3.49

layers, the PCE value of device with ZnO layer is expected to be higher than the PCE value of device with TiO_2 layer [37–40]. Moreover, the optical transmittance measurement indicates that the average transmittance value of the ZnO thin film is considerably higher than the average transmittance value of the TiO_2 thin film in the wavelength range of 400–900 nm as given in Fig. 2a. Since ZnO thin film has a higher optical transmission value than TiO_2 thin film, more photons can reach the photoactive area of the cells in which the ZnO thin film layer used as ESL. High transmittance indicates that more photons are reaching the photoactive layer from the sun in the devices, resulting in high PCE of the solar cells [59]. Based on these reasons and the J-V results, the incorporation of sputtered ZnO layer enables IPSC devices to operate more efficient than incorporation of sputtered TiO_2 layer.

Author's personal copy

Conclusions

In summary, metal oxides of TiO_2 and ZnO thin films in between FTO-coated glass substrates and P3HT:PCBM polymer active layer as an electron selective layer in the IPSC were deposited by using sputtering method. The blended of P3HT:PCBM polymer was fabricated onto FTO/Glass, TiO_2/FTO/Glass and ZnO/FTO/Glass substrates by using spin coater technique. The X-ray diffraction pattern showed that produced metal oxides of TiO_2 and ZnO thin films were polycrystalline structure with the most intense peak positions at 26.7° and 36.6°, respectively. Both films have (101) preferred orientation. The confocal Raman spectrum of P3HT:PCBM polymer photoactive layer demonstrated that the major Raman peak is at 1448 cm^{-1} which is related with C=C symmetric stretching mode. AFM measurements of TiO_2, ZnO and P3HT:PCBM thin film indicated that the prepared samples have average roughness of 9.11 nm, 13.75 nm and 5.60 nm, respectively. The *J–V* characteristics of the IPSC device samples under the illumination without ESL and with sputtered TiO_2 and ZnO electron sellective layers demonstrated a PCE value of 0.13, 2.88 and 3.49% for TiO_2 and ZnO layers, respectively.

The characterization of the crystalline structures, optical properties and the surface morphologies of sputtered TiO_2 and ZnO thin film samples proved that both films are suitable for using as the electron selective layer to insert in between FTO and photoactive polymer layers in IPSCs. However, the photovoltaic performances of cells showed that sputtered ZnO thin film has higher PCE value than sputtered TiO_2 thin film.

Acknowledgements This work was partially supported by The Presidency of Strategy and Budget (Turkey) under the project number of 2016K121220.

Compliance with ethical standards

Conflict of interest The authors declare no competing financial interests.

References

1. Tang CW (1986) Two-layer organic photovoltaic cell. Appl Phys Lett 48:183. https://doi.org/10.1063/1.96937
2. Granström M, Petritsch K, Arias AC, Lux A, Andersson MR, Friend RH (1998) Laminated fabrication of polymeric photovoltaic diodes. Nature 395:257–260. https://doi.org/10.1038/26183
3. Lewis NS (2007) Toward cost-effective solar energy use. Science 315:798. https://doi.org/10.1126/science.1137014
4. Brabec CJ, Sariciftci NS, Hummelen JC (2001) Plastic solar cells. Adv Funct Mater 11:15–26. https://doi.org/10.1002/1616-3028(200102)11:1%3c15:AID-ADFM15%3e3.0.CO;2-A
5. Vezie MS, Few S, Meager I, Pieridou G, Dörling B, Ashraf RS, Goñi AR, Bronstein H, McCulloch I, Hayes SC, Campoy-Quiles M, Nelson J (2016) Exploring the origin of high optical absorption in conjugated polymers. Nat Mater 15:746–753. https://doi.org/10.1038/nmat4645
6. Deng WQ, Goddard WA (2004) Predictions of hole mobilities in oligoacene organic semiconductors from quantum mechanical calculations. J Phys Chem B 108:8614–8621. https://doi.org/10.1021/jp0495848
7. Dennler G, Scharber MC, Brabec CJ (2009) Polymer-fullerene bulk-heterojunction solar cells. Adv Mater 21:1323–1338. https://doi.org/10.1002/adma.200801283

Author's personal copy

8. Kim JY, Lee K, Coates NE, Moses D, Nguyen T-Q, Dante M, Heeger AJ (2007) Efficient tandem polymer solar cells fabricated by all-solution processing. Science 317:222–225. https://doi.org/10.1126/science.1141711
9. Peumans P, Yakimov A, Forrest SR (2003) Small molecular weight organic thin-film photodetectors and solar cells. J Appl Phys 93:3693–3723. https://doi.org/10.1063/1.1534621
10. Mihailetchi VD, Koster LJA, Blom PWM, Melzer C, De Boer B, Van Duren JKJ, Janssen RAJ (2005) Compositional dependence of the performance of poly(p-phenylene vinylene): methanofullerene bulk-heterojunction solar cells. Adv Funct Mater 15:795–801. https://doi.org/10.1002/adfm.200400345
11. Yuan J, Zhang Y, Zhou L, Zhang G, Yip H-L, Lau T-K, Lu X, Zhu C, Peng H, Johnson PA, Leclerc M, Cao Y, Ulanski J, Li Y, Zou Y (2019) Single-junction organic solar cell with over 15% efficiency using fused-ring acceptor with electron-deficient core. Joule 3:1140–1151. https://doi.org/10.1016/j.joule.2019.01.004
12. Meng L, Zhang Y, Wan X, Li C, Zhang X, Wang Y, Ke X, Xiao Z, Ding L, Xia R, Yip H-L, Cao Y, Chen Y (2018) Organic and solution-processed tandem solar cells with 173% efficiency. Science 361:1094–1098. https://doi.org/10.1126/science.aat2612
13. Hoppe H, Sariciftci NS (2004) Organic solar cells: an overview. J Mater Res 19:1924–1945. https://doi.org/10.1557/JMR.2004.0252
14. Van Bavel SS, Bärenklau M, De With G, Hoppe H, Loos J (2010) P3HT/PCBM bulk heterojunction solar cells: impact of blend composition and 3D morphology on device performance. Adv Funct Mater 20:1458–1463. https://doi.org/10.1002/adfm.200902247
15. Yang X, Loos J, Veenstra SC, Verhees WJH, Wienk MM, Kroon JM, Michels MAJ, Janssen RAJ (2005) Nanoscale Morphology of High-Performance Polymer Solar Cells. Nano Lett 5:579–583. https://doi.org/10.1021/nl048120i
16. Shi J, Lv L, Zhou W, Zhang L (2014) Improvement of the photovoltaic properties for P3HT:PCBM system annealed at the temperature in liquid crystalline regions induced by liquid crystal molecules. Polym Bull 71:2963–2979. https://doi.org/10.1007/s00289-014-1233-z
17. Brabec CJ (2004) Organic photovoltaics: technology and market. Sol Energy Mater Sol Cells 83:273–292. https://doi.org/10.1016/j.solmat.2004.02.030
18. Lu Y, Wang Y, Feng Z, Ning Y, Liu X, Lü Y, Hou Y (2012) Temperature-dependent morphology evolution of P3HT:PCBM blend solar cells during annealing processes. Synth Met 162:2039–2046. https://doi.org/10.1016/j.synthmet.2012.10.012
19. Yu G, Gao J, Hummelen JC, Wudl F, Heeger AJ (1995) Polymer photovoltaic cells: enhanced efficiencies via a network of ınternal donor-acceptor heterojunctions. Science 270:1789–1791. https://doi.org/10.1126/science.270.5243.1789
20. Hu J, Wu Z, Wei H, Song T, Sun B (2012) Effects of ZnO fabricating process on the performance of inverted organic solar cells. Org Electron 13:1171–1177. https://doi.org/10.1016/j.orgel.2012.03.021
21. He Z, Zhong C, Huang X, Wong W-Y, Wu H, Chen L, Su S, Cao Y (2011) Simultaneous enhancement of open-circuit voltage, short-circuit current density, and fill factor in polymer solar cells. Adv Mater 23:4636–4643. https://doi.org/10.1002/adma.201103006
22. Zhu F, Chen X, Zhou L, Zhou J, Yang J, Huang S, Sun Z (2014) Dependence of the performance of inverted polymer solar cells on thickness of an electron selective ZnO layer deposited by magnetron sputtering. Thin Solid Films 551:131–135. https://doi.org/10.1016/j.tsf.2013.11.096
23. Kawano K, Pacios R, Poplavskyy D, Nelson J, Bradley DDC, Durrant JR (2006) Degradation of organic solar cells due to air exposure. Sol Energy Mater Sol Cells 90:3520–3530. https://doi.org/10.1016/J.SOLMAT.2006.06.041
24. Klimov E, Li W, Yang X, Hoffmann GG, Loos J (2006) Scanning near-field and confocal Raman microscopic investigation of P3HT-PCBM systems for solar cell applications. Macromolecules 39:4493–4496. https://doi.org/10.1021/ma052590x
25. Zhou Y, Cheun H, Potscavage WJ Jr, Fuentes-Hernandez C, Kim S-J, Kippelen B (2010) Inverted organic solar cells with ITO electrodes modified with an ultrathin Al_2O_3 buffer layer deposited by atomic layer deposition. J Mater Chem 20:6189. https://doi.org/10.1039/c0jm00662a
26. Kim H-K, Chung K-B, Kal J (2019) Comparison of ZnO buffer layers prepared by spin coating or RF magnetron sputtering for application in inverted organic solar cells. J. Alloys Compd. 778:487–495. https://doi.org/10.1016/j.jallcom.2018.11.240
27. Gullu HH, Yildiz DE, Kocyigit A, Yıldırım M (2020) Electrical properties of Al/PCBM:ZnO/p-Si heterojunction for photodiode application. J. Alloys Compd. 827:154279. https://doi.org/10.1016/j.jallcom.2020.154279

Author's personal copy

28. Wang J-C, Weng W-T, Tsai M-Y, Lee M-K, Horng S-F, Perng T-P, Kei C-C, Yu C-C, Meng H-F (2010) Highly efficient flexible inverted organic solar cells using atomic layer deposited ZnO as electron selective layer. J Mater Chem 20:862–866. https://doi.org/10.1039/B921396A
29. Xiong J, Yang B, Zhou C, Yang J, Duan H, Huang W, Zhang X, Xia X, Zhang L, Huang H, Gao Y (2014) Enhanced efficiency and stability of polymer solar cells with TiO2 nanoparticles buffer layer. Org Electron 15:835–843. https://doi.org/10.1016/j.orgel.2014.01.024
30. Kırbıyık Ç, Büyükçelebi S, Yiğit MZ, Can M, Kara K, Kuş M, Kara DA (2019) Improving the performance of inverted polymer solar cells through modification of compact TiO_2 layer by different boronic acid functionalized self-assembled monolayers. Appl Surf Sci 479:177–184. https://doi.org/10.1016/j.apsusc.2019.01.268
31. Hong S, Han A, Lee EC, Ko K-W, Park J-H, Song H-J, Han M-H, Han C-H (2015) A facile and low-cost fabrication of TiO_2 compact layer for efficient perovskite solar cells. Curr Appl Phys 15:574–579. https://doi.org/10.1016/j.cap.2015.01.028
32. Sun H, Weickert J, Hesse HC, Schmidt-Mende L (2011) UV light protection through TiO2 blocking layers for inverted organic solar cells. Sol Energy Mater Sol Cells 95:3450–3454. https://doi.org/10.1016/j.solmat.2011.08.004
33. Jiang Z, Yang D, Wang N, Zhang F, Zhao B, Tan S, Zhang J (2013) Inverted polymer solar cells with TiO_2 electron extraction layers prepared by magnetron sputtering. Sci China Chem 56:1573–1577. https://doi.org/10.1007/s11426-013-4901-1
34. Ge S, Xu H, Wang W, Cao R, Wu Y, Xu W, Zhu J, Xue F, Hong F, Xu R, Xu F, Wang L, Huang J (2016) The improvement of open circuit voltage by the sputtered TiO2 layer for efficient perovskite solar cell. Vacuum 128:91–98. https://doi.org/10.1016/j.vacuum.2016.03.013
35. Alparslan Z, Kösemen A, Örnek O, Yerli Y, San SE (2011) Based organic hybrid solar cells with doping. Int J Photoenergy 2011:1–8. https://doi.org/10.1155/2011/734618
36. Hau SK, Yip H-L, Baek NS, Zou J, O'Malley K, Jen AK-Y (2008) Air-stable inverted flexible polymer solar cells using zinc oxide nanoparticles as an electron selective layer. Appl Phys Lett 92:253301. https://doi.org/10.1063/1.2945281
37. Yildiz A, Lisesivdin SB, Kasap M, Mardare D (2008) Electrical properties of TiO_2 thin films. J Non Cryst Solids 354:4944–4947. https://doi.org/10.1016/j.jnoncrysol.2008.07.009
38. Nowotny J, Radecka M, Rekas M (1997) Semıconductıng properties of undoped TiO_2. J Phys Chem Solids 58:927–937. https://doi.org/10.1016/S0022-3697(96)00204-1
39. Vai AT, Kuznetsov VL, Dilworth JR, Edwards PP (2014) UV-induced improvement in ZnO thin film conductivity: a new in situ approach. J. Mater. Chem. C. 2:9643–9652. https://doi.org/10.1039/C4TC01749H
40. Gençyilmaz O (2016) Hydrothermal synthesis of ZnO films and characterization Anadolu Univ. J Sci Technol A 17:660. https://doi.org/10.18038/aubtda.267254
41. Schumann S, Da Campo R, Illy B, Cruickshank AC, McLachlan MA, Ryan MP, Riley DJ, McComb DW, Jones TS (2011) Inverted organic photovoltaic devices with high efficiency and stability based on metal oxide charge extraction layers. J Mater Chem 21:2381–2386. https://doi.org/10.1039/C0JM03048A
42. Andersson A, Johansson N, Bröms P, Yu N, Lupo D, Salaneck WR (1998) Fluorine tin oxide as an alternative to ındium tin oxide in polymer LEDs. Adv Mater 10:859–863. https://doi.org/10.1002/(SICI)1521-4095(199808)10:11%3c859:AID-ADMA859%3e3.0.CO;2-1
43. Helander MG, Greiner M, Tang WM, Helander MG, Greiner MT, Wang ZB, Lu ZH (2011) Work function of fluorine doped tin oxide. Artic J Vac Sci Technol A. https://doi.org/10.1116/1.3525641
44. Beek WJE, Slooff LH, Wienk MM, Kroon JM, Janssen RAJ (2005) Hybrid solar cells using a zinc oxide precursor and a conjugated polymer. Adv Funct Mater 15:1703–1707. https://doi.org/10.1002/adfm.200500201
45. Bahar M, Gholami M, Azim-Araghi ME (2014) Sol–gel synthesized Titania nanoparticles deposited on porous polycrystalline silicon: improved carbon dioxide sensor properties. Mater Sci Semicond Process 26:491–500. https://doi.org/10.1016/j.mssp.2014.05.035
46. Iyengar P, Das C, Balasubramaniam KR (2017) Photoelectrochemical performance of NiO-coated ZnO–CdS core-shell photoanode. J Phys D 50:1001. https://doi.org/10.1088/1361-6463/aa5875
47. Kumar KDA, Valanarasu S, Jeyadheepan K, Kim HS, Vikraman D (2018) Evaluation of the physical, optical, and electrical properties of SnO2: F thin films prepared by nebulized spray pyrolysis for optoelectronics. J Mater Sci 29:3648–3656. https://doi.org/10.1007/s10854-017-8295-2

Author's personal copy

48. Jeyasubramanian K, Gokul Raja TS, Purushothaman S, Kumar MV, Sushmitha I (2017) Supercapacitive performances of MnO_2 nanostructures grown on hierarchical Cu nano leaves via electrodeposition. Electrochim Acta 227:401–409. https://doi.org/10.1016/j.electacta.2017.01.044
49. Sagasti A, Bouropoulos N, Kouzoudis D, Panagiotopoulos A, Topoglidis E, Gutiérrez J (2017) Nanostructured ZnO in a Metglas/ZnO/hemoglobin modified electrode to detect the oxidation of the hemoglobin simultaneously by cyclic voltammetry and magnetoelastic resonance. Materials. https://doi.org/10.3390/ma10080849
50. Chin H-S, Chao L-S (2013) The effect of thermal annealing processes on structural and photoluminescence of zinc oxide thin film. J Nanomater 2013:1–8. https://doi.org/10.1155/2013/424953
51. Yoon KH, Choi J, Lee D (1997) Characteristics of ZnO thin films deposited onto A1/Si substrates by rf magnetron sputtering. Thin Solid Films 302:116–121
52. Falke S, Eravuchira P, Materny A, Lienau C (2011) Raman spectroscopic identification of fullerene inclusions in polymer/fullerene blends. J Raman Spectrosc 42:1897–1900. https://doi.org/10.1002/jrs.2966
53. Kumar S, Kumar M, Rathi S, Yadav A, Upadhyaya A, Gupta SK, Singh A (2018) Study of P3HT/PCBM morphology using Raman spectroscopy. AIP Conf Proc 1953:100074. https://doi.org/10.1063/1.5033010
54. Keru G, Ndungu P, Mola G, Nyamori V (2015) Bulk heterojunction solar cell with nitrogen-doped carbon nanotubes in the active layer: effect of nanocomposite synthesis technique on photovoltaic properties. Materials (Basel) 8:2415–2432. https://doi.org/10.3390/ma8052415
55. Candan İ, Parlak M, Erçelebi Ç (2019) PbS quantum dot enhanced p-CIGS/n-Si heterojunction diode. J Mater Sci 30:2127–2135. https://doi.org/10.1007/s10854-018-0484-0
56. Paci B, Generosi A, Albertini VR, Spyropoulos GD, Stratakis E, Kymakis E (2012) Enhancement of photo/thermal stability of organic bulk heterojunction photovoltaic devices via gold nanoparticles doping of the active layer. Nanoscale 4:7452–7459. https://doi.org/10.1039/c2nr32799f
57. Tsoi WC, James DT, Kim JS, Nicholson PG, Murphy CE, Bradley DDC, Nelson J, Kim JS (2011) The nature of in-plane skeleton Raman modes of P3HT and their correlation to the degree of molecular order in P3HT:PCBM blend thin films. J Am Chem Soc 133:9834–9843. https://doi.org/10.1021/ja2013104
58. Guo TF, Wen TC, Lvovich Pakhomov G, Chin XG, Liou SH, Yeh PH, Yang CH (2008) Effects of film treatment on the performance of poly(3-hexylthiophene)/soluble fullerene-based organic solar cells. Thin Solid Films 516:3138–3142. https://doi.org/10.1016/j.tsf.2007.08.066
59. Nasuno Y, Kohama N, Nishimura K, Hayakawa T, Taniguchi H, Shimizu M (2006) Effect of perforated transparent electrodes on light transmittance and light scattering in substrates used for microcrystalline silicon thin-film solar cells. Appl Phys Lett 88:071909. https://doi.org/10.1063/1.2176857

Publisher's Note Springer Nature remains neutral with regard to jurisdictional claims in published maps and institutional affiliations.